




Probing de novo sphingolipid metabolism in mammalian cells utilizing mass spectrometry^S

Justin M. Snider,^{*,†,§} Ashley J. Snider,^{†,§,***} Lina M. Obeid,^{†,§,***} Chiara Luberto,^{1,§,††} and Yusuf A. Hannun^{1,†,§}

Molecular and Cellular Biology and Biochemistry and Structural Biology Graduate Program,^{*} Departments of Medicine[†] and Physiology and Biophysics,^{††} and Stony Brook Cancer Center,[§] Stony Brook University, Stony Brook, NY; and Northport Veterans Affairs Medical Center,^{***} Northport, NY

ORCID IDs: 0000-0002-2839-8888 (L.M.O.); 0000-0003-3349-3369 (Y.A.H.)

Abstract Sphingolipids constitute a dynamic metabolic network that interconnects several bioactive molecules, including ceramide (Cer), sphingosine (Sph), Sph 1-phosphate, and Cer 1-phosphate. The interconversion of these metabolites is controlled by a cohort of at least 40 enzymes, many of which respond to endogenous or exogenous stimuli. Typical probing of the sphingolipid pathway relies on sphingolipid mass levels or determination of the activity of individual enzymes. Either approach is unable to provide a complete analysis of flux through sphingolipid metabolism, which, given the interconnectivity of the sphingolipid pathway, is critical information to identify nodes of regulation. Here, we present a one-step in situ assay that comprehensively probes the flux through de novo sphingolipid synthesis, post serine palmitoyltransferase, by monitoring the incorporation and metabolism of the 17 carbon dihydro sphingosine precursor with LC/MS. Pulse labeling and analysis of precursor metabolism identified sequential well-defined phases of sphingolipid synthesis, corresponding to the activity of different enzymes in the pathway, further confirmed by the use of specific inhibitors and modulators of sphingolipid metabolism.  This work establishes precursor pulse labeling as a practical tool for comprehensively studying metabolic flux through de novo sphingolipid synthesis and complex sphingolipid generation.—Snider, J. M., A. J. Snider, L. M. Obeid, C. Luberto, and Y. A. Hannun. **Probing de novo sphingolipid metabolism in mammalian cells utilizing mass spectrometry.** *J. Lipid Res.* 2018. 59: 1046–1057.

Supplementary key words flux • 17CdhSph • d17dhSph • 17 carbon dihydro sphingosine

Sphingolipid metabolites play a myriad of roles in cellular biology, including apoptosis, cell-cycle arrest, differentiation, migration, proliferation, and senescence (1–4). In addition to signaling, sphingolipids constitute an important component of cellular membranes, where they maintain the integrity of their structure and organization. In turn, these sphingolipid-mediated biologies have been implicated in metabolism, neurodevelopment, inflammation, cancer, and several other physiological and pathological processes (5–10).

Because of their regulatory role in these critical processes, the synthesis and turnover of sphingolipids appears to be tightly regulated. As shown in **Fig. 1**, de novo synthesis begins in the endoplasmic reticulum (ER) with the condensation of serine and palmitoyl-CoA by way of serine palmitoyltransferase (SPT), the rate-limiting step in this pathway. The 3-keto-dihydro sphingosine product of this reaction is quickly reduced to generate dhSph. N-acylation of dhSph to form dihydroceramide (dhCer) is achieved via one of six (dihydro)ceramide synthases (CerSs), each with affinity for specific chain lengths of fatty acyl-CoAs. Beyond this, dhCer is desaturated via dhCer desaturase (DeS) into ceramide (Cer), which can then be transferred from the ER to the Golgi to form complex sphingolipids, the most abundant of which are SM and hexosylceramide (HexCer). The transport of Cer from ER to Golgi is

This work was supported by National Institutes of Health Grant R35 GM118128 (Y.A.H.), and National Cancer Institute Grant P01-CA97132 (Y.A.H., L.M.O., C.L.). This work was performed with assistance from Cold Spring Harbor Laboratories Mass Spectrometry Shared Resource, which is supported by the Cancer Center Support Grant 5P30CA045508. The content is solely the responsibility of the authors and does not necessarily represent the official views of the National Institutes of Health. The authors declare no conflicts of interest.

Manuscript received 7 November 2017 and in revised form 26 March 2018.

Published, JLR Papers in Press, April 2, 2018

DOI <https://doi.org/10.1194/jlr.D081646>

Abbreviations: BFA, brefeldin A; CDase, ceramidase; Cer, ceramide; CerS, ceramide synthase; DeS, dihydroceramide desaturase; dhCer, dihydroceramide; dhSph, dihydro sphingosine; d17Cer, d17ceramide; d17dhSph, d17dihydro sphingosine (precursor); d17S-1-P, d17sphingosine-1-phosphate; d17Sph, d17sphingosine (17 carbon backbone sphingosine); ER, endoplasmic reticulum; FB1, fumonisin B1; HexCer, hexosylceramide; 4-HPR, fenretinide; MPB, mobile phase B; SK, sphingosine kinase; SMS, SM synthase; Sph, sphingosine; SPT, serine palmitoyltransferase.

¹To whom correspondence should be addressed.

e-mail: Yusuf.Hannun@stonybrookmedicine.edu (Y.A.H.);

Chiara.Luberto@stonybrookmedicine.edu (C.L.)

^SThe online version of this article (available at <http://www.jlr.org>) contains a supplement.

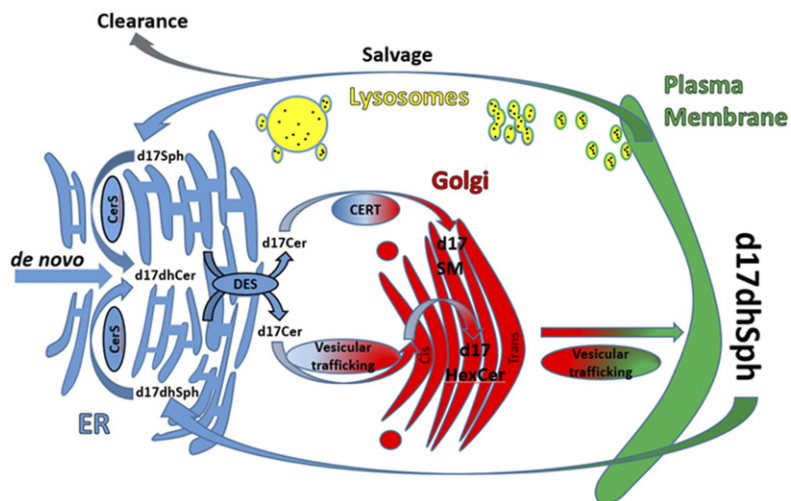


Fig. 1. Cellular map of d17sphingolipid metabolism. This is a simplified scheme of the pathways of d17dh-Sph metabolism. Major organelles in sphingolipid processing are represented, along with the localization of the major enzymes and metabolites measured with this methodology.

achieved by the action of the transfer protein, CERT, which preferentially couples Cer transport to SM synthesis (11), as well as via vesicular trafficking, which delivers Cer for the synthesis of both HexCer and SM. HexCer then serves as a substrate for the synthesis of more complex glycosphingolipids (12). These complex sphingolipids are then transported to the plasma membrane and are ultimately fated to undergo degradation through hydrolytic pathways, mostly in the lysosomes, culminating with the release of sphingosine (Sph) through the action of acid ceramidase (CDase). At this point, Sph flips and/or is transported across the lysosomal membranes where it can either be phosphorylated through Sph kinase (SK) activity or reintegrated into the sphingolipid network through CerS activity via the salvage pathway.

Most sphingolipids can be metabolized via the activity of multiple enzymes, which are often localized in specific sub-cellular compartments, and these compartments contain various sphingomyelinases, CDases, CerSs, and cerebrosidases. Thus, regulation of these enzymes can create discrete cellular pools of sphingolipids, thereby complicating the evaluation of sphingolipid metabolism and participation in specific regulatory pathways.

Indeed, evidence for the involvement of sphingolipids in biologic processes relies on studies focusing on specific enzymes of sphingolipid metabolism and/or changes of mass levels of bioactive sphingolipids. However, typical lipid analyses examine total cell lysates to evaluate mass levels. Thus, while these approaches have revealed regulated modulation of bioactive sphingolipids, they lack the ability to provide a comprehensive understanding of the dynamic changes occurring throughout the sphingolipid network. This becomes critical due to the complexity of the sphingolipid network creating a need to establish more specific methods to probe these fluxes in their entirety.

Such needs have been partially met by the use of exogenous lipids, inhibitors, radiolabeled lipids, fluorophores, and odd-chained lipids, which have all been employed to interrogate single enzymes or segments in the sphingolipid metabolic pathway (13–21). Moreover, assays that utilize thin-layer chromatography for the detection of the

labeled lipids are unable to discriminate the variations in the N-acyl chain length, which can play a role in sphingolipid biology (22–24). One approach to dissecting cellular pools of lipids is to utilize a label such as an unnatural 17 carbon sphingoid base for flux analysis monitored by LC/MS/MS (25, 26). Assays of this nature have been utilized to assess CerS and SK activities measuring the conversion of d17sphingosine (d17Sph) into d17ceramide (d17Cer) or d17sphingosine-1-phosphate (d17S-1-P), respectively (13, 27, 28).

To address the need for a comprehensive analysis of de novo sphingolipid biosynthesis that could quantitatively capture the flux through the different enzymatic phases of the pathway in cells, we set out to optimize the use of d17dihydrosphingosine (d17dhSph; precursor) in MCF-7 breast cancer cells. Mass spectrometer transitions and LC retention times were established for 17C metabolites, including d17dhCer, d17Cer, d17HexCer, d17SM, and 17 carbon sphingoid bases. The odd-chain backbone incorporation into the different metabolites was assessed at different concentrations and time points to generate pulse labeling parameters that spanned de novo synthesis. We then identified discrete temporal phases of enzyme activities through the de novo pathway and utilized modulators of sphingolipid metabolic steps to further define these enzymatic phases. This study lays the groundwork for precursor as a practical tool to decipher the intricate flux through de novo sphingolipid metabolism.

MATERIALS AND METHODS

Chemicals and reagents

Synthetic sphingolipid reference standards (Cer 13:1/16:0, Cer 13:1/22:0, d17Sph, d17dhSph, d17S-1-P, Cer d17:1/16:0, Cer d17:1/24:1, SM d18:1/18:1, SM d18:1/17, GluCer d18:1/18:1, GluCer d18:1/C17, Sph, dhSph, S-1-P, Cer d18:1/16:0, Cer d18:1/24, Cer d18:1/24:1Cer, SM d18:1/16:0, SM d18:1/24:1, GluCer d18:1/16:0, and GluCer d18:1/24:1) were either synthesized at the Medical University of South Carolina Lipidomics Shared Resource Core or acquired from Avanti Polar Lipids Inc.

(Alabaster, AL). Analytical grade solvents from Burdick and Jackson (Muskegon, MI) were used unless otherwise noted. Extraction solvent A consisted of 2-propanol/ethyl acetate (15:85 v/v) and was utilized in the extraction of medium samples, while extraction solvent B consisted of ethyl acetate/2-propanol/water (60:30:10, v/v) and was utilized for cell/tissue extractions.

Cell lines and cell culture

MCF-7 human breast adenocarcinoma cells were obtained from ATCC (Manassas, VA) and maintained in RPMI medium (Gibco-Invitrogen, Carlsbad, CA) containing 10% (v/v) FBS. Cells were maintained in a humidified incubator at 37°C with 5% CO₂.

Pulse labeling with d17dhSph

MCF-7 cells were plated in a 10 cm dish at approximately 30% confluence (400,000 cells) for 48 h prior to labeling with precursor; 23 h after plating, the medium was changed to RPMI containing 2% FBS. Label was added to a final concentration of 500 nM (or as indicated in the specific experiment) from a 10 μM stock in ethanol. Cells were incubated for the indicated time points and harvested utilizing direct extraction techniques previously established by Bielawski et al. (29).

Inhibitor treatments

MCF-7 cells were grown and labeled as in the pulse section. When the medium was changed to RPMI with 2% FBS, either GT-11 (1 μM), fenretinide (4-HPR) (2.5 μM), or fumonisin B1 (FB1) (25 μM) was added. For brefeldin A (BFA)-treated cells, the reagent was added directly to the medium to a final concentration of 24 μM for 1 h before pulse began. Abbreviated pulses were utilized when possible to focus only on the relevant phases.

Analysis by HPLC/MS/MS

Chromatographic separation was achieved utilizing a Thermo Accela HPLC (Thermo Fisher Scientific, Waltham, MA). Conditions were optimized employing a Peek Scientific C-8 column (3 μm particle, 4.6 × 150 mm). A column temperature of 45°C maximized intensity and integrity of analytes while maintaining baseline separation. Mobile phase A consisted of MS grade water containing 0.2% formic acid and 1 mM ammonium formate (pH 5.6), and mobile phase B (MPB) consisted of MS grade methanol containing 0.2% formic acid and 1 mM ammonium formate (pH 5.6). Chromatographic conditions were as follows: upon sample injection, the gradient was constant for 2 min at 82% MPB, then increased to 90% MPB by 4 min, then increased to 98% MPB by 10 min, and 98% MPB was sustained until 28 min, at which point MPB was reduced to 82% by 30 min, and then reequilibrated for 5 min, for a total gradient of 35 min. For SM analysis, an abbreviated gradient was utilized. Briefly, upon sample injection, the gradient was ramped from 90% MPB to 99% MPB over the first 7 min, then maintained at 99% MPB until 17 min into the gradient, at which point the gradient was returned to 90% MPB within 1 min and allowed to equilibrate until 21 min. Detection was accomplished utilizing a Thermo Scientific Quantum Access triple quadrupole mass spectrometer (Thermo Fisher Scientific) equipped with an electrospray ion source operating in positive ion and multiple reaction monitoring modes. The ESI source was operated at 400°C vaporizer temperature and 300°C capillary temperature in positive ionization mode with a spray voltage of 3,500 V. Gasses were set at 40, 5, and 10 for sheath, ion sweep, and auxiliary gases, respectively. MS detection of labeled lipids was accomplished using transitions described in supplemental Table S1 (29). Due to limitations in standards availability and instrumentation (scan speeds versus sensitivity when detecting large numbers

of mass transitions), only the major species of N-acyl chain length were monitored.

Statistical analysis

One-way ANOVA, two-way ANOVA, and Student's *t*-test were utilized for statistical analysis in GraphPad Prism software. Bonferroni's posttest was applied for multiple comparisons for both one-way and two-way ANOVA analysis.

RESULTS

Development of LC/MS conditions for acquisition and quantitation of d17-labeled sphingolipids

Chromatographic conditions and MS transitions for d17 sphingoid bases, d17dhCers, and d17Cers have been established in the literature (25, 29), yet expanding these studies to include complex sphingolipids has not been done. Only a single standard for each of d17HexCer and d17SM was commercially available, thus retention times for all d17HexCers and d17SMs were calculated utilizing a comparison of SM d18:1/17:0 to SM d18:1/18:1 and HexCer standards. The retention times for SM d18:1/17:0 differed from SM d18:1/18:1 by 30 s. To generate retention times for putative d17SM and d17HexCer analytes, MCF-7 cells were labeled with 1 μM precursor for 2 h. When compared with their 18 carbon SM (standard) counterparts, SM d17:1/16:0, d17:1/C24:1, and d17:1/24 were assigned to peaks corresponding to an average retention time shift of 25, 45, and 50 s, respectively. Similar shifts of 30, 45, and 50 s were observed for HexCer d17:1/16:0, d17:1/24:1, and d17:1/24, respectively. MS transitions were calculated utilizing 18 carbon backbone standards of the corresponding N-acyl chain length to 17 carbon analytes of interest. The minus water fragmentation product (*m/z* - 18) was by far the most abundant product ion generated, thus the corresponding 17 carbon product ions were calculated and utilized for quantitation. The characteristic fragment ion of *m/z* 250.3 was utilized as a diagnostic peak corresponding to the 17 carbon sphingoid backbone (supplemental Table S1).

Incorporation of precursor into de novo sphingolipid metabolism

Pulse labeling experiments to probe sphingolipid metabolic flux have been traditionally performed with radioactive isotopes or fluorescent lipids; however, these assays can suffer from a lack of sensitivity and specificity in acyl chain length. These limitations are circumvented by the use of a 17 carbon Sph as a probe in conjunction with MS analysis of 17 carbon sphingolipid metabolites (25, 29). To gather a general picture of the metabolism of precursor into sphingolipids and to determine appropriate parameters (dose and time) for subsequent experiments, MCF-7 cells were first labeled for 1 h with increasing doses (50–1,000 nM) of precursor, and the resulting 17 carbon sphingolipid products were monitored by MS. The uptake of the exogenous precursor label into cells (Fig. 2A) and its conversion into d17dhCer and d17Cers (Fig. 2B, C) occurred in a dose-dependent manner. However, below the concentration

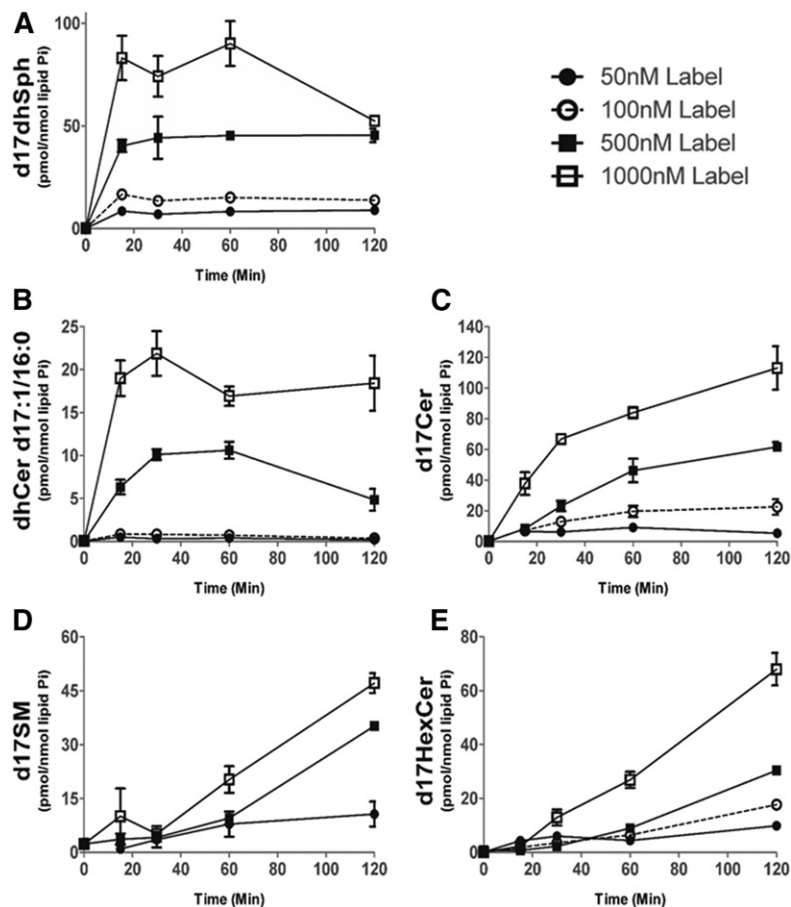


Fig. 2. d17dhSph dose-dependent label incorporation. MCF-7 cells were labeled with 50, 100, 500, or 1,000 nM of 17 carbon backbone dihydrosphingosine (precursor) (17CdhSph) for a 120 min pulse, then harvested and analyzed with HPLC/MS/MS. Intracellular levels of d17dhSph (A), dhCer d17:0/16:0 (B), d17Cer (C), d17SM (50 nM not acquired) (D), and d17HexCer (E) are presented ($n = 2$). Data are expressed as mean \pm SD.

of 500 nM, we could not achieve accurate quantitation of d17dhCer during the CerS phase (Fig. 2B). Because of these limitations in sensitivity, we selected the lowest concentration that allowed accurate quantitation across d17 metabolites (500 nM). The metabolism of 500 nM precursor did not contribute significantly to total cellular mass of SM and HexCer over the 120 min pulse, but generated approximately four times more labeled dhCer and Cer (supplemental Fig. S1) compared with endogenous levels; though at the 120 min time point, the incorporation profiles of individual labeled molecular species matched the endogenous ones (supplemental Fig. S2), supporting the experimental legitimacy of utilizing a 500 nM concentration of precursor for our studies. Lastly, while the 1,000 nM concentrations of precursor demonstrated more robust incorporation into 17 carbon metabolites (Fig. 2), exogenous treatment with sphingoid bases in the low micromolar range can exert significant biological effects (30), thus we utilized 500 nM of precursor for subsequent labeling studies, as this dose was optimally incorporated into sphingolipids, allowing clear detection of metabolites, even at very early time points, without apparent biological effects occurring during the duration of the labeling.

Next, a time course of precursor label uptake and incorporation was performed. MCF-7 cells were labeled with 500 nM of precursor for up to 120 min. Precursor label reached a maximal intracellular concentration within 5 min of addition to the media, which corresponded to approxi-

mately 5% of extracellular precursor, and remained stable for the rest of the incubation time (Fig. 3A, B). The amount of precursor label in the media was measured and found to slowly decrease over the 120 min time course, yet still represented over 60% of the initial label (Fig. 3C). Reciprocally, the incorporation of label into combined cellular pools of precursor, d17dhCer, d17Cer, d17SM, and d17HexCer, for the major N-acyl species (C16, C24:1, C24) was measured and found to show a progressive increase over this time course (Fig. 3C). These data indicate that extracellular precursor label was in excess throughout the pulse and that intracellular precursor was readily available for metabolism.

CerS phase occurs between 2 and 15 min into the pulse

In order to determine flux rates through the sphingolipid network, we next utilized precursor to define consecutive enzymatic reactions of the de novo biosynthetic pathway, past the SPT/3-keto-dhSph reductase reactions. MCF-7 cells were labeled with 500 nM of precursor for 120 min, and sphingolipid metabolism was assessed via ESI/MS/MS. The maximal rate of precursor label incorporation into d17dhCer was observed during the first 15 min of the pulse (Fig. 4A), thus a best fit line was constructed utilizing time points between 2 and 15 min (Fig. 4B). For MCF-7 cells, the major species of N-acyl chain length incorporated via the six different CerSs included dhCer d18:0/16:0, dhCer d18:0/24:1, and dhCer d18:0/24. It was observed that the maximum rate of precursor incorporation into the different

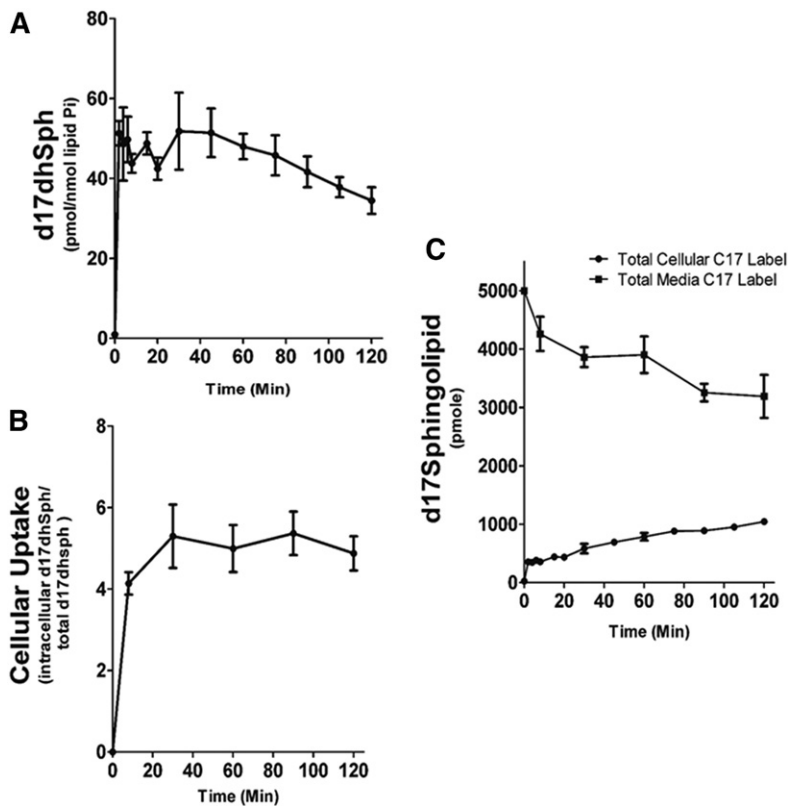


Fig. 3. The 17dhSph cellular uptake. MCF-7 cells were labeled with 500 nM d17dhSph. Cells were harvested at the indicated time points and analyzed with HPLC/MS/MS. A: Intracellular levels of d17dhSph. B: Intracellular d17dhSph given as a percentage of extracellular d17dhSph levels. C: Extracellular (media) d17dhSph after indicated times incubated with cells and the combined intracellular levels of d17dhSph, d17dhCer, d17Cer, d17SM, and d17HexCer. Data are expressed as mean \pm SD, $n = 3$.

N-acyl chain lengths of dhCer occurred between 2 and 15 min (supplemental Fig. S3). Therefore, the slope of the line in Fig. 4B represents the rate of d17dhCer production and corresponds to the total activity of the CerS enzymes. This rate is calculated at 0.61 pmol of d17dhCer per nanomole of lipid Pi per minute (pmol/nmol Pi/min) (Table 1).

As CerSs are the first enzymes in de novo sphingolipid synthesis to utilize precursor, the conversion of precursor into d17dhCer via CerS activity commenced almost immediately with the x-intercept reading at 1.2 min (Fig. 4B). Therefore, the interval of time between 2 and 15 min defined what we termed the “CerS phase”.

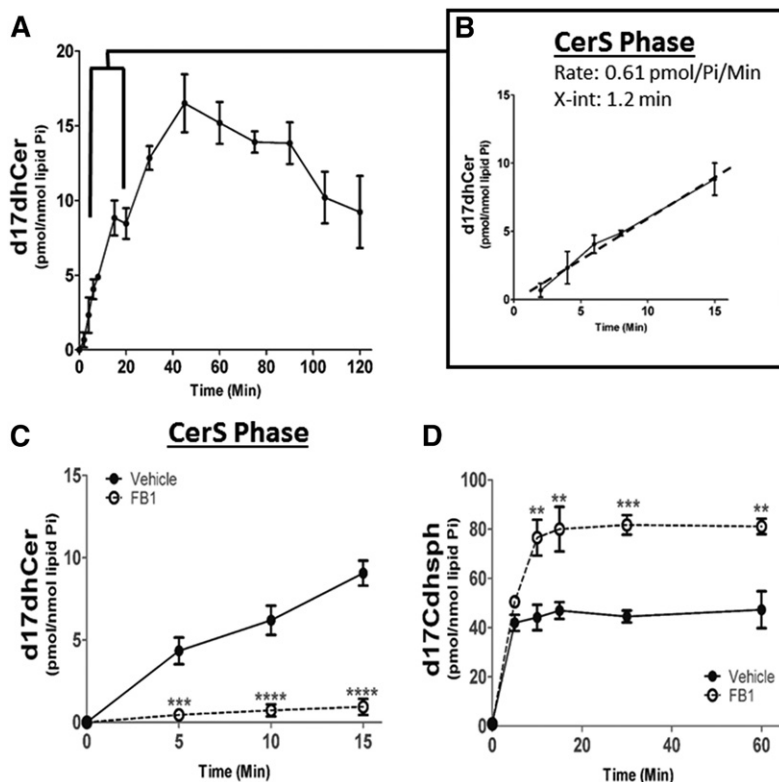


Fig. 4. Identification of CerS phase during d17dhSph pulse. MCF-7 cells were labeled with 500 nM d17dhSph and labeled sphingolipids analyzed by LC/MS/MS. A: d17dhCer levels throughout the full 120 min pulse. B: Inset represents CerS phase between 2 and 15 min with calculated line of best fit. C, D: Cells were treated with 25 μ M FBI for 24 h prior to pulse; CerS phase (d17dhCer) (C) and intracellular levels (D) of d17dhSph were analyzed. Data are expressed as mean \pm SD, $n = 3$. ** $P < 0.01$, *** $P < 0.001$, and **** $P < 0.0001$ as compared with vehicle.

TABLE 1. In situ sphingolipid enzymatic activity rates

Phase	Vehicle (pmol/nmol Pi/min)	FB1 (pmol/nmol Pi/min)	GT-11 (pmol/nmol Pi/min)	BFA (pmol/nmol Pi/min)
CerS (total)	0.61 (100%)	0.061 (10%)	0.60 (98%)	0.54 (89%)
DeS	0.85 (100%)	NI	0.026 (3%)	0.24 (28%)
HexCer synthesis	0.37 (100%)	NI	NI	0.39 (105%)
SM synthesis	0.39 (100%)	NI	NI	1.2 ^a (308%)

Rates are the calculated as slope of label incorporation into the product analyte for a given enzymatic reaction during the time frames (phases) established in Figs. 4–6. Units are picomoles of labeled product per nanomole of lipid Pi per minute. Percent vehicle is also given. NI, no incorporation.

^aRate for adjusted phase.

To further confirm the involvement of CerS during the first phase of precursor metabolism, we tested the effect of the potent CerS inhibitor, FB1, on d17dhCer formation (31). MCF-7 cells were pretreated with 25 μ M of FB1 for 24 h prior to labeling with precursor, and labeled sphingolipids were assessed via LC/MS/MS. Pretreatment with FB1 decreased CerS activity by 90% during the CerS phase with minimal accumulation of d17dhCer detected (Fig. 4C, Table 1). Interestingly, the precursor substrate of the CerS accumulated rapidly upon inhibition by FB1 (Fig. 4D), demonstrating that initial label incorporation is CerS dependent. Further metabolism of the precursor label was similarly reduced in the subsequent DeS, HexCer, and SM metabolic phases (Table 1).

DeS phase occurs between 20 and 60 min into the pulse

The product of CerS activity, dhCer, is next desaturated via DeS (32) to produce d17Cer. The maximum rate of d17Cer formation occurred between 20 and 60 min (Fig. 5A). Again, a line was constructed for this interval, the x-intercept was at 6.2 min and a rate of 0.85 pmol/nmol

Pi/min for Cer generation was calculated, establishing the “DeS phase” (Fig. 5B, Table 1). In agreement with the higher activity of DeS (0.85 pmol/nmol Pi/min) compared with CerS (0.61 pmol/nmol Pi/min), labeled DeS substrate (d17dhCer) began to decline at 45 min (Fig. 4A), during the DeS phase. As we did not observe changes in the rates of formation of the different N-acyl species, the DeS phase is being shown as total d17Cer (supplemental Fig. S3).

To confirm the identification of the DeS phase, the effects of two well-established DeS inhibitors, GT-11 (33) and 4-HPR (34), were tested on production of d17Cer. MCF-7 cells were treated with 1 μ M of GT-11 or 2.5 μ M of 4-HPR, and metabolism of the 17 carbon label was measured with LC/MS/MS. Both DeS inhibitors resulted in increased levels of labeled d17dhCer during the DeS phase (Fig. 5C); for example, d17dhCer increased by 279 \pm 39% with GT-11 and by 128 \pm 17% with 4-HPR at the 60 min time point, corresponding to the end of the DeS phase, indicating a backup in the DeS substrate (Fig. 5C). This was accompanied by a near total inhibition of formation of the d17Cer products (Fig. 5D, Table 1), such that the rate of d17Cer

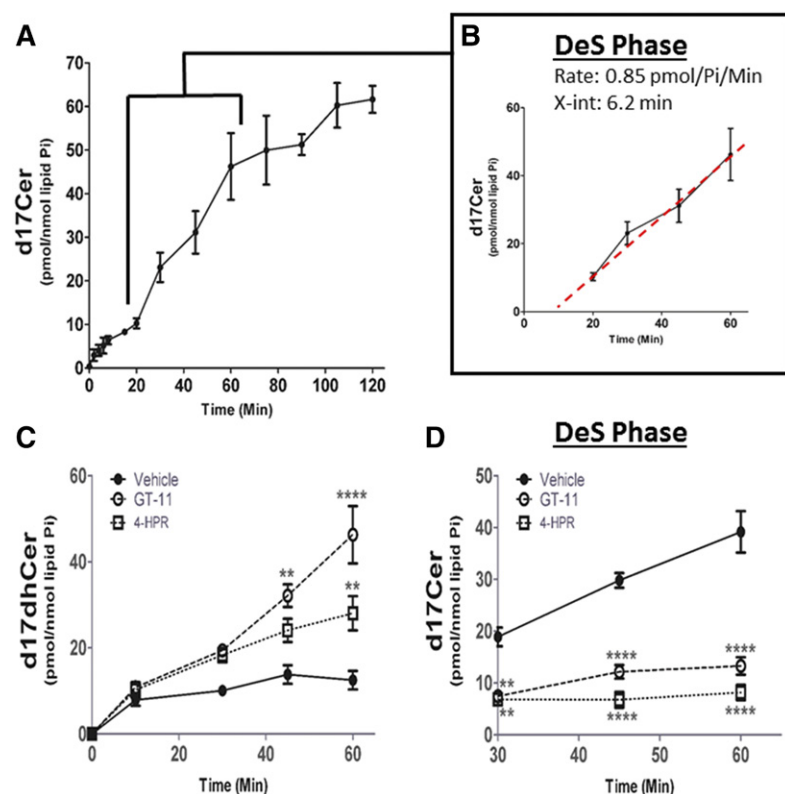


Fig. 5. Identification of DeS phase during d17dhSph pulse. MCF-7 cells were labeled with 500 nM d17dhSph and labeled sphingolipids analyzed by LC/MS/MS. A: d17Cer flux throughout the full 120 min pulse. B: Inset represents DeS phase between 20 and 60 min with calculated line of best fit. C, D: Cells were treated with 1 μ M GT-11 or 2.5 μ M 4-HPR for 24 h prior to pulse; d17Cer (C) and d17dhCer (D) were analyzed. Data are expressed as mean \pm SD, n = 3. ** P < 0.01, and **** P < 0.0001 as compared with vehicle.

formation displayed a 97% decrease with GT-11 and a 98% decrease with 4-HPR during the DeS phase (Fig. 5D). There was no detectable label incorporation in d17SM or d17HexCer in either condition (Table 1). Importantly, generation of the DeS substrate remained unaffected during the CerS phase (Fig. 5C, Table 1). The selective inhibition of d17Cer production by GT-11 and 4-HPR and the fact that the rate of d17dhCer remained unaffected upon treatment with the DeS inhibitors support the correct assignment of the CerS and DeS phases during the metabolic labeling with precursor.

Complex sphingolipid metabolic phases occur after 60 min of precursor pulse

In order for Cer to be converted into complex sphingolipids, it first has to be transported from the ER to the Golgi. This transfer represents a metabolic “fork in the road”, in which the CERT protein transfers Cer from ER to Golgi, preferentially for generation of SM, while vesicular transfer favors the incorporation of Cer into HexCer (Fig. 1). In accordance with the literature (35, 36) and the spatial separation of the ER and Golgi, the generation of appreciable amounts of labeled complex sphingolipids only appeared after 20–45 min into the pulse (Fig. 6). The maximal rate of d17SM synthesis occurred between 60 and 120 min (Fig. 6A). Analysis of kinetics during this phase demonstrated a rate of synthesis of 0.39 pmol/nmol Pi/min (Fig. 6B, Table 1) with an x-intercept that indicates synthesis began at 35 min. Consistent with C16SM being the most abundant SM molecular species in this cell type in steady state conditions (supplemental Fig. S2) (37), SM d17:1/16:0 was the predominant molecular species of SM produced during the 60–120 min period of the pulse designated the “SM synthesis phase” (supplemental Fig. S2, Fig. 6). HexCer synthesis exhibited a similar delay to that of SM (x-intercept of 28 min) and a maximal rate of 0.37 pmol/nmol Pi/min between 60 and 120 min, establishing the “HexCer synthesis phase” (Fig. 6C, D; Table 1). As we did not observe changes in the rates of formation of the different N-acyl species, the HexCer synthesis phase is being shown as total d17HexCer. Taken together, these data establish rates of synthesis for complex 17 carbon-labeled sphingolipids and the time interval at which Cer is delivered from the ER to the next biosynthetic step in the Golgi.

As a means to investigate the delay in the initial label incorporation into complex sphingolipids, BFA was utilized. BFA is an antibiotic that has been shown to induce fusion of the Golgi and ER (38), producing an increase in SM synthase (SMS) activity, while having lesser effects on HexCer synthesis (39). MCF-7 cells were pretreated with a 24 μ M dose of BFA for 1 h, and d17-labeled sphingolipids were assessed with ESI/MS/MS. The results showed a dramatic decrease in the delay of incorporation for labeled SM, which began almost immediately (Fig. 6E). Moreover, there was an increase in the maximum rate of synthesis to 1.2 pmol/nmol Pi/min occurring within the first 10 min of the pulse (Fig. 6E, Table 1). No significant change in the rate of synthesis of d17HexCer was observed, but the initiation of incorporation was reduced by 20 min, when calculated

using a best fit line during the normal HexCer synthesis phase (Fig. 6F, Table 1). Finally, BFA caused the substrate for both pathways, d17Cer, to be utilized at a much greater rate; such that by the end of the 120 min pulse, incorporation of the label into d17Cer had decreased by $50 \pm 15\%$ in BFA-treated cells (Fig. 6G). Taken together, these data verify the assessment that the delay in generation of labeled complex sphingolipids is due to the limiting step in the transfer of Cer between the ER and Golgi.

Sphingoid bases and phosphates

The phosphorylation of Sph into S-1-P by SK1 and -2 is a very important step in sphingolipid-mediated signaling, as well as clearance of sphingolipids from cellular pools. While d17S-1-P was below the detection limit during the labeling time, d17dhS-1-P, the direct product of label phosphorylation, paralleled the cellular levels of precursor with an almost immediate increase followed by a plateau (Fig. 7A). Because the precursor substrate was still in excess, these data suggest that dhS-1-P achieves steady state levels very rapidly. The generation of Sph from dhSph first requires conversion into Cer and then the action of CDases. The generation of d17Sph appeared to reach a maximum rate between 20 and 60 min, with a rate of synthesis of 0.016 pmol/nmol Pi/min (Fig. 7B). This activity paralleled the generation of the CDase substrate, d17Cer, during the DeS phase in the ER. Taken together, these data establish the discrete intervals during the pulse that reflect the activities of individual enzymes in de novo sphingolipid synthesis (post-SPT).

DISCUSSION

In this study, we set out to define and optimize precursor as a tool to study flux through the de novo sphingolipid pathway. Based on rates of label incorporation into 17 carbon sphingolipid metabolites during a 120 min precursor pulse, we identified discrete phases of synthesis of sphingolipid metabolites that correspond to the enzymatic activities for CerS, DeS, HexCer, and SM synthesis in MCF-7 breast cancer cells. These kinetic results also agree with what is currently known about the subcellular localization of de novo synthesis of sphingolipids (36, 38–40). Notably, all results were acquired from a single-step approach utilizing a 17 carbon sphingoid label that demonstrates very similar biochemical properties to the endogenous substrates; as such, all obtained metabolic rates are comparable to those of natural sphingolipids. Taken together, these results establish the use of d17dhSph as a novel tool for probing and distinguishing multiple de novo sphingolipid enzymatic activities simultaneously.

The first phase to be detected was that of the CerS. This CerS phase was established based on the formation of d17dhCer, and was initiated almost immediately upon addition of labeled precursor to media, proceeding linearly for 15 min (up to 40 min) into the pulse. It should be noted in this context that uptake of precursor was detected at the very earliest time point we could measure, and remained

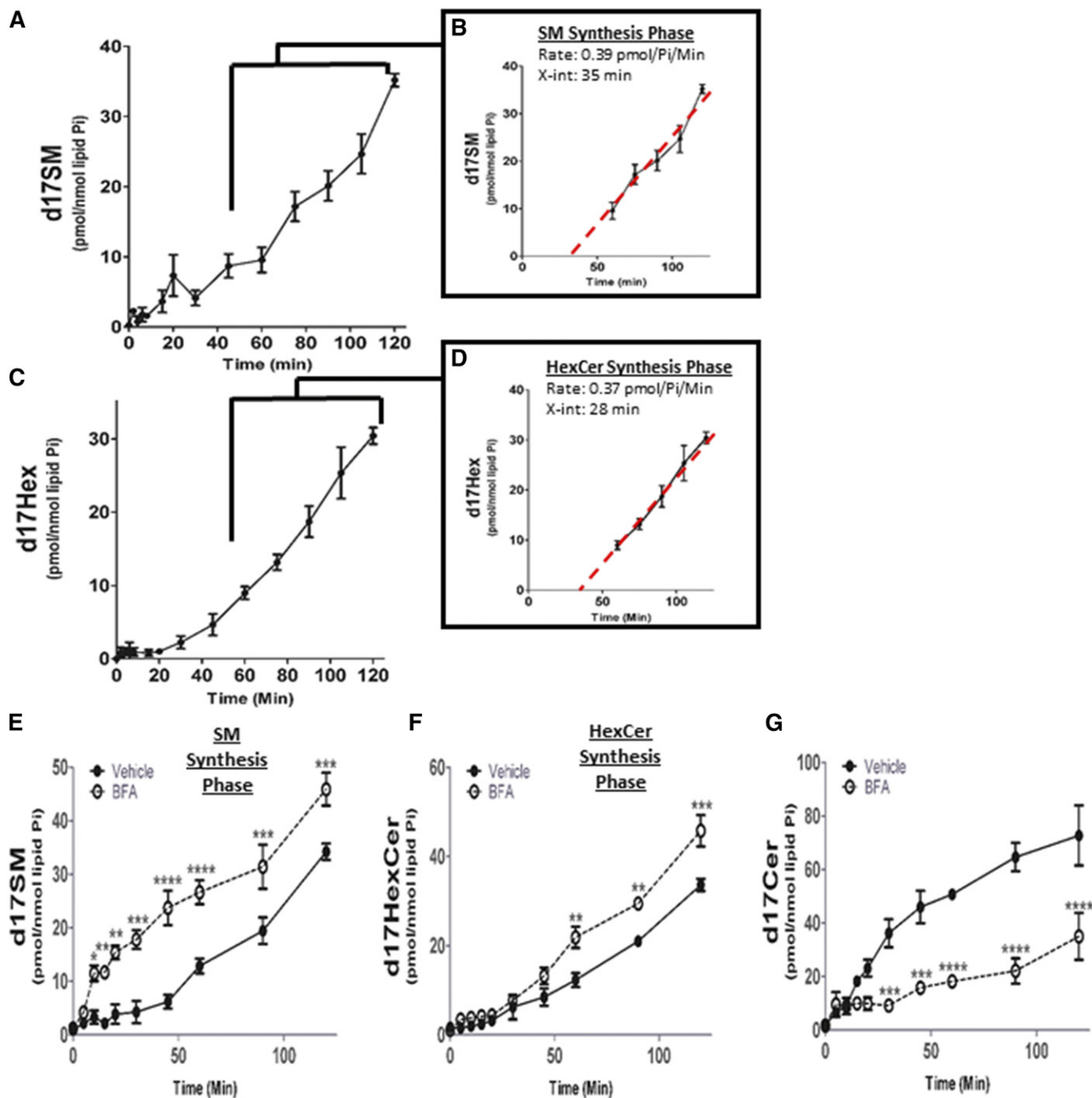


Fig. 6. Identification of complex sphingolipid synthetic phases from de novo-generated d17Cer during pulse. MCF-7 cells were labeled with 500 nM d17dhSph. Cells were harvested at the indicated time points and analyzed with HPLC/MS/MS. A: d17SM levels throughout the full 120 min pulse. B: Inset represents SM synthesis phase between 60 and 120 min with calculated line of best fit. C: d17HexCer levels throughout the full 120 min pulse. D: Inset represents HexCer synthesis phase between 60 and 120 min with calculated line of best fit. E–G: Cells were treated with 25 μ M BFA for 1 h prior to pulse and d17Cer (E), d17SM (F), and d17HexCer (G) were analyzed for the entire 120 min pulse. Data are expressed as mean \pm SD, $n = 3$. * $P < 0.05$, ** $P < 0.01$, *** $P < 0.001$, and **** $P < 0.0001$ as compared with vehicle.

steady throughout the course of this experimental approach. The incorporation of 17 carbon backbone sphingoid bases by CerS is well-studied (18, 28, 41), though mostly utilizing d17Sph in the context of the salvage pathway. Jin et al. (41) incubated cells with 1 μ M of precursor for 30 min to measure changes in CerS enzymatic activity in response to Compound C, a potent inhibitor of AMP-activated protein kinase. Importantly, changes in label

incorporation paralleled those in mRNA levels of CerS, and were consistent with the observed changes in endogenous Cer levels in response to CerS induction by Compound C. Our data demonstrate that more robust results may be achieved by monitoring d17dhCer directly during the CerS phase in the first 15 min of the pulse. In another study, d17Sph was utilized to measure CerS activity in BMK cells (18). As d17Sph forms d17Cer directly without the

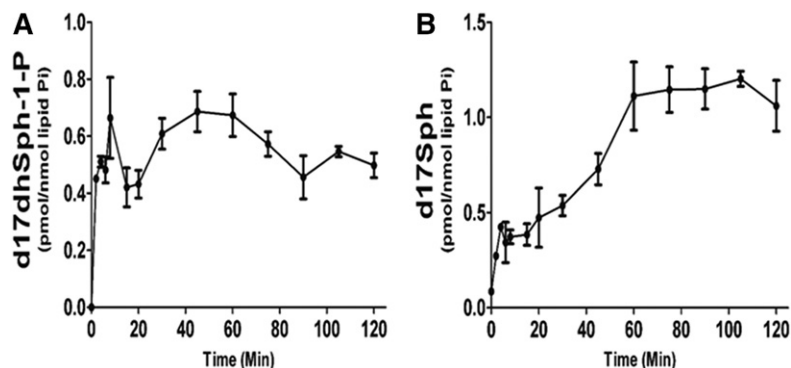


Fig. 7. Time-dependent incorporation of d17dhSph label into sphingoid base and phosphate. MCF-7 cells were labeled with 500 nM d17dhSph. Cells were harvested at relevant time points and analyzed with HPLC/MS/MS. A: d17dhSph-1-P levels during entire 120 min pulse. B: d17Sph levels throughout the full 120 min pulse. Data are expressed as mean \pm SD, $n = 3$.

need for desaturation, the authors were able to monitor CerS-dependent label incorporation within ~ 13 min of label addition. Notably, both in vitro and in situ assays utilizing d17Sph aligned to indicate regulation of specific isoforms of CerS via BAK protein in the context of apoptosis. Thus, either d17Sph or precursor labels are amenable to measuring CerS activity, as long as the proper time points (phases) and substrates are considered.

While CerS activity is considered the major form of sphingoid base N-acylation, reverse CDase activity, which is FB1 insensitive, has also been implicated in Cer production (16, 42). Thus, as a means of determining reverse CDase contribution to d17dhCer pools, we utilized the CerS inhibitor, FB1, to more accurately define enzymatic contribution to the CerS phase. As reported by El-Bawab et al. (16), reverse CDase activity has very low affinity toward dhSph, thus it was expected that there would be very little contribution from reverse CDase activity. Indeed, we observed a $90 \pm 5\%$ decrease in d17dhCer levels at the end of the CerS phase (15 min) upon FB1 treatment (Fig. 4C), indicating that CerS activity is the overwhelming Cer synthesizing mechanism and that it could be accurately monitored during this period of the pulse.

Interestingly, an increase in the precursor substrate for CerS was observed upon FB1 treatment (Fig. 4D). In this context, it was important to note that during the 120 min pulse, precursor levels appeared to be maintained by the cell at 5% of the media concentration (Fig. 3C). With CerS inhibition, this number doubled to almost 10% only during the CerS phase, then remained stable for the remainder of the pulse (Fig. 4D). The reason for this is unknown at present, but may represent saturated mechanisms of uptake, clearance, and/or feedback.

This approach also defines a discrete DeS phase by monitoring the formation of d17Cer following the production of d17dhCer. This phase is the next step in the de novo metabolism of the 17 carbon label (Fig. 1), and it produced the maximum rate of labeled product between 20 and 60 min into the pulse. Utilizing D-erythro-C12-dihydro pyridinium bromide as an analog of dhCer, Apraiz et al. (43) demonstrated that DeS inhibition by 4-HPR could be determined at 60 min following label addition. Indeed, in our study, DeS inhibition with either GT-11 or 4-HPR was utilized to further demonstrate the d17Cer generated during the 20–60 min window of time to be DeS dependent (Fig. 5D). Of note, the CerS phase remained unaffected by the

treatments, as it was only during the DeS phase that d17dhCer began to accumulate (Fig. 5C), further validating the 2–15 min time points selected for CerS. While there currently are adequate substrates for measuring DeS activity in vitro and in situ, this is the first time, to our knowledge, that this label has been utilized to monitor flux between the CerS and DeS.

Analysis of the kinetics of formation and loss of d17dhCer also provides further insights into the actions of both CerS and DeS. Rapid N-acylation of exogenous sphingoid bases has been observed (13, 18, 28), but of particular interest in our study was the peak in 17 carbon label incorporation into d17dhCer pools at 45 min, followed by a significant decrease. This decrease in the d17dhCer can be interpreted by considering the rates established during the phases responsible for dhCer generation and utilization. Michaelis-Menten kinetics have been established for both enzymes involved in dhCer metabolism. In vitro V_{max} values established in the literature consistently range in the picomoles per minute per milligram for CerS activity (44, 45). Faster DeS activity has been measured in vitro utilizing both dhCerC6NBD (46) and D-erythro-C12-dihydro pyridinium bromide (34) as substrates, with V_{max} values of 1.71 and 3.16 nmol/min/mg, respectively. However, it is difficult to extrapolate these in vitro rates to cells, as the in vitro rates are dependent on the purity of the enzyme preparation, whereas cell studies can also be affected by factors present in cells and not accounted for in vitro, including the cellular location of the enzymes, regulatory subunits, and cofactors. In our study, under basal conditions, the cellular CerS rate was calculated to be 0.61 pmol/nmol Pi/min, while DeS demonstrated a faster rate of 0.85 pmol/nmol Pi/min (Table 1). Thus, it is not surprising that during the DeS phase, the d17dhCer substrate begins to decrease. Additionally, when DeS activity was inhibited (Fig. 5C), the production of d17dhCer continued past the 45 min peak observed in vehicle, maintaining the initial maximal rate of synthesis. These results indicate that CerS activity is not inhibited by accumulation of its product (at least during the interval of time considered) and that the relative activity of DeS versus CerS is the critical determinant of the amounts of d17dhCer produced.

Importantly, the generation of d17Sph, which requires the action of CDases, occurred with a maximal rate at the same time interval in the pulse as DeS activity (Figs. 5B, 7B), indicating that CDase activity could be measured with

this approach as well. It is important to consider that there are three alkaline CDases (ACER 1–3), two of which have distinct localization to either the ER or Golgi. Thus, the time window during the pulse in which d17Sph is being generated can indicate which ACERs are likely responsible for Cer metabolism. In unperturbed MCF-7 cells, it appears that rapid turnover of newly synthesized Cer occurs immediately upon generation in the ER, thus either ACER 1 and/or ACER 3 activity is likely responsible. CDase activities have been monitored via fluorescent and natural substrate in vitro (47, 48), but this is the first time an in situ flux assay has been performed to measure ER CDase activity rates.


The final phases to be detected with this approach were the subsequent synthesis of both SM and HexCer, which were delayed until 60–120 min. The lag observed in initial incorporation of the label into complex sphingolipids corresponds quite closely to established knowledge on the rate of transfer for Cer from the ER to the Golgi, with initial incorporation calculated in the current study at 35 min for SM and 28 min for HexCer. Indeed, previous observations utilizing either NBD-C6-Cer (35) or a photoactivable and clickable analog of Sph (36), indicated that exogenously added sphingolipid requires at least 30 min to begin incorporation into Golgi pools of sphingolipid. Of note, these studies both observed initial localization of labeled lipid in a different compartment from the Golgi, thus transfer of labeled metabolites was required. These earlier studies had the obvious limitation of not knowing how well the exogenous analogs mimicked the function of endogenous sphingolipids. Given that the d17Cer generated during the pulse closely mimics natural Cer substrate in biophysical properties as well as localization, it should more accurately reflect processing of endogenous substrates. Moreover, dissection of flux through these two pathways by examining endogenous levels has been complicated by the fact that both metabolites are at relatively high concentrations in the cell when compared with their biosynthetic precursor Cer, with the latter also serving as product of hydrolysis of SM and HexCer. Thus, small changes in SM and HexCer can affect Cer levels substantially. The current approach allows the detection of small changes in these synthetic pathways.

Vesicular trafficking and protein-mediated transport via the action of CERT are required for generation of both HexCer and SM (Fig. 1). Our data demonstrate that generation of d17SM and d17HexCer occur at relatively the same rate and with similar initial incorporation of our label (Fig. 6). Thus, utilizing BFA allowed the deconvolution of these two fundamentally different forms of lipid trafficking. Previously, it has been reported that BFA treatment enhanced incorporation of short-chain Cers into short-chain SM, while the conversion into short-chain HexCer was unchanged (39, 49). In our study, BFA decreased the time the d17Cer took to reach SMS enzymes from 35 min to 5 min, suggesting that 30 min is approximately the time necessary for Cer to reach SMS in the Golgi from the ER (Fig. 6E). Moreover, the rate of flux for d17SM synthesis was increased by 300% during BFA treatment (Fig. 6E). As both substrates for SM synthesis, phosphatidylcholine and Cer, are synthesized in the ER, there is a large excess of

substrate available to the SMS enzyme upon BFA treatment and the increase in the rate of SM synthesis under these conditions indicates that substrate limitation occurs in the Golgi (49). In our conditions, treatment with BFA initiated the synthesis of HexCer at an earlier time point (8.6 min), while the maximal rate of synthesis remained unchanged, reflecting the fact that the substrate availability for GCS is a function of trafficking of the label from the ER to the Golgi and not of the Cer availability. On the other hand, it has been shown that the formation of glycosphingolipids could be driven under high glucose conditions, thus pointing to UDP-glucose as the rate limiting factor in this metabolic step (50). Interestingly, these results highlight a substantial difference between GCS and SMS utilization of Cer substrate transferred from the ER.

Phosphorylation of Sph has been probed in a few studies utilizing 17 carbon sphingoid bases as a substrate for SK activity, though no consensus has been established in the literature for assay parameters (27, 51–53). Importantly, our study would suggest that steady state levels of d17dhSph-1-P are reached very rapidly (within 2 min, Fig. 7A) making it unfeasible to probe flux through SK. Thus, studies assessing conversion of precursor into d17dhSph-1-P as a measure of SK activity at steady state are actually measuring the balance between the synthesis of d17dhSph-1-P and its catabolism.

One limitation of this approach is the exclusion from the analysis of the first two steps of sphingolipid metabolism, SPT and reductase. Probing SPT activity would require labeling with either serine or palmitate metabolites (20) that are not unique to the sphingolipid pathway. Moreover, SPT can utilize the additional amino acids, glycine and alanine, as well as additional fatty acyl-CoAs, such as stearoyl-CoA and myristoyl-CoA. Thus, evaluation of SPT activity itself would then require a range of different precursors.

In summary, we have established precursor as a one-step practical molecular label for a comprehensive analysis of sphingolipid metabolic flux in situ. The phases ascribed based on the 120 min pulse of precursor accurately depict flux through de novo sphingolipid generation through complex sphingolipid synthesis. Thus, this tool can now be applied to known modulators of the sphingolipid network to gain a better understanding of regulation of key enzymes in the pathway. 

The authors would like to thank Dr. Darryl Pappin and Dr. Ashutosh Singh for their assistance with analytical methods and small molecule chromatography. The authors would also like to thank the staff and personnel of the Stony Brook University Lipidomics Core Facility (Dr. John Haley, Izolda Mileva, and Rob Rieger).

REFERENCES

1. Hannun, Y. A., and L. M. Obeid. 2008. Principles of bioactive lipid signalling: lessons from sphingolipids. *Nat. Rev. Mol. Cell Biol.* **9**: 139–150.
2. Obeid, L. M., C. M. Linaudic, L. A. Karolak, and Y. A. Hannun. 1993. Programmed cell death induced by ceramide. *Science*. **259**: 1769–1771.

3. Jayadev, S., B. Liu, A. E. Bielawska, J. Y. Lee, F. Nazaire, Pushkareva MYu, L. M. Obeid, and Y. A. Hannun. 1995. Role for ceramide in cell cycle arrest. *J. Biol. Chem.* **270**: 2047–2052.
4. Merrill, A. H., Jr. 2002. De novo sphingolipid biosynthesis: a necessary, but dangerous, pathway. *J. Biol. Chem.* **277**: 25843–25846.
5. Holland, W. L., and S. A. Summers. 2008. Sphingolipids, insulin resistance, and metabolic disease: new insights from in vivo manipulation of sphingolipid metabolism. *Endocr. Rev.* **29**: 381–402.
6. Li, X., K. A. Becker, and Y. Zhang. 2010. Ceramide in redox signaling and cardiovascular diseases. *Cell. Physiol. Biochem.* **26**: 41–48.
7. Haughey, N. J., V. V. Bandaru, M. Bae, and M. P. Mattson. 2010. Roles for dysfunctional sphingolipid metabolism in Alzheimer's disease neuropathogenesis. *Biochim. Biophys. Acta.* **1801**: 878–886.
8. Gangoiti, P., L. Camacho, L. Arana, A. Ouro, M. H. Granado, L. Brizuela, J. Casas, G. Fabriás, J. L. Abad, A. Delgado, et al. 2010. Control of metabolism and signaling of simple bioactive sphingolipids: implications in disease. *Prog. Lipid Res.* **49**: 316–334.
9. Meyers-Needham, M., S. Ponnusamy, S. Gencer, W. Jiang, R. J. Thomas, C. E. Senkal, and B. Ogretmen. 2012. Concerted functions of HDAC1 and microRNA-574-5p repress alternatively spliced ceramide synthase 1 expression in human cancer cells. *EMBO Mol. Med.* **4**: 78–92.
10. Pettus, B. J., K. Kitatani, C. E. Chalfant, T. A. Taha, T. Kawamori, J. Bielawski, L. M. Obeid, and Y. A. Hannun. 2005. The coordination of prostaglandin E2 production by sphingosine-1-phosphate and ceramide-1-phosphate. *Mol. Pharmacol.* **68**: 330–335.
11. Hanada, K., K. Kumagai, S. Yasuda, Y. Miura, M. Kawano, M. Fukasawa, and M. Nishijima. 2003. Molecular machinery for non-vesicular trafficking of ceramide. *Nature.* **426**: 803–809.
12. D'Angelo, G., E. Polishchuk, G. Di Tullio, M. Santoro, A. Di Campli, A. Godi, G. West, J. Bielawski, C. C. Chuang, A. C. van der Spoel, et al. 2007. Glycosphingolipid synthesis requires FAPP2 transfer of glucosylceramide. *Nature.* **449**: 62–67.
13. Spassieva, S., J. G. Seo, J. C. Jiang, J. Bielawski, F. Alvarez-Vasquez, S. M. Jazwinski, Y. A. Hannun, and L. M. Obeid. 2006. Necessary role for the Lag1p motif in (dihydro)ceramide synthase activity. *J. Biol. Chem.* **281**: 33931–33938.
14. Villani, M., M. Subathra, Y. B. Im, Y. Choi, P. Signorelli, M. Del Poeta, and C. Luberto. 2008. Sphingomyelin synthases regulate production of diacylglycerol at the Golgi. *Biochem. J.* **414**: 31–41.
15. Venkataraman, K., and A. H. Futerman. 2001. Comparison of the metabolism of L-erythro- and L-threo-sphinganine and ceramides in cultured cells and in subcellular fractions. *Biochim. Biophys. Acta.* **1530**: 219–226.
16. El Bawab, S., H. Birbes, P. Roddy, Z. M. Szulc, A. Bielawska, and Y. A. Hannun. 2001. Biochemical characterization of the reverse activity of rat brain ceramidase. A CoA-independent and fumonisin B1-insensitive ceramide synthase. *J. Biol. Chem.* **276**: 16758–16766.
17. van Echten, G., H. Iber, H. Stotz, A. Takatsuki, and K. Sandhoff. 1990. Uncoupling of ganglioside biosynthesis by Brefeldin A. *Eur. J. Cell Biol.* **51**: 135–139.
18. Siskind, L. J., T. D. Mullen, K. Romero Rosales, C. J. Clarke, M. J. Hernandez-Corbacho, A. L. Edinger, and L. M. Obeid. 2010. The BCL-2 protein BAK is required for long-chain ceramide generation during apoptosis. *J. Biol. Chem.* **285**: 11818–11826.
19. Martínez-Montañés, F., and R. Schneider. 2016. Tools for the analysis of metabolic flux through the sphingolipid pathway. *Biochimie.* **130**: 76–80.
20. Merrill, A. H., Jr., E. Wang, and R. E. Mullins. 1988. Kinetics of long-chain (sphingoid) base biosynthesis in intact LM cells: effects of varying the extracellular concentrations of serine and fatty acid precursors of this pathway. *Biochemistry.* **27**: 340–345.
21. Hu, W., J. Bielawski, F. Samad, A. H. Merrill, Jr., and L. A. Cowart. 2009. Palmitate increases sphingosine-1-phosphate in C2C12 myotubes via upregulation of sphingosine kinase message and activity. *J. Lipid Res.* **50**: 1852–1862.
22. Funato, K., and H. Riezman. 2001. Vesicular and nonvesicular transport of ceramide from ER to the Golgi apparatus in yeast. *J. Cell Biol.* **155**: 949–959.
23. Ogawa, K., Y. Fujiwara, K. Sugamata, and T. Abe. 1988. Thin-layer chromatography of neutral glycosphingolipids: an improved simple method for the resolution of GlcCer, GalCer, LacCer and Ga2Cer. *J. Chromatogr. A.* **426**: 188–193.
24. Reggiori, F., E. Canivenc-Gansel, and A. Conzelmann. 1997. Lipid remodeling leads to the introduction and exchange of defined ceramides on GPI proteins in the ER and Golgi of *Saccharomyces cerevisiae*. *EMBO J.* **16**: 3506–3518.
25. Spassieva, S., J. Bielawski, V. Anelli, and L. M. Obeid. 2007. Combination of C(17) sphingoid base homologues and mass spectrometry analysis as a new approach to study sphingolipid metabolism. *Methods Enzymol.* **434**: 233–241.
26. Martínez-Montañés, F., and R. Schneider. 2016. Following the flux of long-chain bases through the sphingolipid pathway in vivo using mass spectrometry. *J. Lipid Res.* **57**: 906–915.
27. Anelli, V., C. R. Gault, A. J. Snider, and L. M. Obeid. 2010. Role of sphingosine kinase-1 in paracrine/transcellular angiogenesis and lymphangiogenesis in vitro. *FASEB J.* **24**: 2727–2738.
28. Senkal, C. E., S. Ponnusamy, M. J. Rossi, J. Bialewski, D. Sinha, J. C. Jiang, S. M. Jazwinski, Y. A. Hannun, and B. Ogretmen. 2007. Role of human longevity assurance gene 1 and C18-ceramide in chemotherapy-induced cell death in human head and neck squamous cell carcinomas. *Mol. Cancer Ther.* **6**: 712–722.
29. Bielawski, J., J. S. Pierce, J. Snider, B. Rembiesa, Z. M. Szulc, and A. Bielawska. 2009. Comprehensive quantitative analysis of bioactive sphingolipids by high-performance liquid chromatography-tandem mass spectrometry. *Methods Mol. Biol.* **579**: 443–467.
30. Riboni, L., A. Prinetti, R. Bassi, P. Viani, and G. Tettamanti. 1998. The effects of exogenous sphingosine on Neuro2a cells are strictly related to the overall capacity of cells to metabolize sphingosine. *J. Biochem.* **124**: 900–904.
31. Wang, E., W. P. Norred, C. W. Bacon, R. T. Riley, and A. H. Merrill, Jr. 1991. Inhibition of sphingolipid biosynthesis by fumonisins. Implications for diseases associated with *Fusarium moniliforme*. *J. Biol. Chem.* **266**: 14486–14490.
32. Michel, C., G. van Echten-Deckert, J. Rother, K. Sandhoff, E. Wang, and A. H. Merrill, Jr. 1997. Characterization of ceramide synthase. A dihydroceramide desaturase introduces the 4,5-trans-double bond of sphingosine at the level of dihydroceramide. *J. Biol. Chem.* **272**: 22432–22437.
33. Triola, G., G. Fabriás, and A. Llebaria. 2001. Synthesis of a cyclopropane analogue of ceramide, a potent inhibitor of dihydroceramide desaturase. *Angew. Chem. Int. Ed. Engl.* **40**: 1960–1962.
34. Rahmaniyan, M., R. W. Curley, Jr., L. M. Obeid, Y. A. Hannun, and J. M. Kravka. 2011. Identification of dihydroceramide desaturase as a direct in vitro target for fenretinide. *J. Biol. Chem.* **286**: 24754–24764.
35. Lipsky, N. G., and R. E. Pagano. 1983. Sphingolipid metabolism in cultured fibroblasts: microscopic and biochemical studies employing a fluorescent ceramide analogue. *Proc. Natl. Acad. Sci. USA.* **80**: 2608–2612.
36. Haberkant, P., F. Stein, D. Höglinger, M. J. Gerl, B. Brügger, P. P. Van Veldhoven, J. Krijgsveld, A. C. Gavin, and C. Schultz. 2016. Bifunctional sphingosine for cell-based analysis of protein-sphingolipid interactions. *ACS Chem. Biol.* **11**: 222–230.
37. Kumagai, K., S. Yasuda, K. Okemoto, M. Nishijima, S. Kobayashi, and K. Hanada. 2005. CERT mediates intermembrane transfer of various molecular species of ceramides. *J. Biol. Chem.* **280**: 6488–6495.
38. Lippincott-Schwartz, J., L. C. Yuan, J. S. Bonifacino, and R. D. Klausner. 1989. Rapid redistribution of Golgi proteins into the ER in cells treated with brefeldin A: evidence for membrane cycling from Golgi to ER. *Cell.* **56**: 801–813.
39. Capasso, S., L. Sticco, R. Rizzo, M. Pirozzi, D. Russo, N. A. Dathan, F. Campelo, J. van Galen, M. Hölttä-Vuori, G. Turacchio, et al. 2017. Sphingolipid metabolic flow controls phosphoinositide turnover at the trans-Golgi network. *EMBO J.* **36**: 1736–1754.
40. Gault, C. R., L. M. Obeid, and Y. A. Hannun. 2010. An overview of sphingolipid metabolism: from synthesis to breakdown. *Adv. Exp. Med. Biol.* **688**: 1–23.
41. Jin, J., T. D. Mullen, Q. Hou, J. Bielawski, A. Bielawska, X. Zhang, L. M. Obeid, Y. A. Hannun, and Y. T. Hsu. 2009. AMPK inhibitor Compound C stimulates ceramide production and promotes Bax redistribution and apoptosis in MCF7 breast carcinoma cells. *J. Lipid Res.* **50**: 2389–2397.
42. Okino, N., X. He, S. Gatt, K. Sandhoff, M. Ito, and E. H. Schuchman. 2003. The reverse activity of human acid ceramidase. *J. Biol. Chem.* **278**: 29948–29953.
43. Apraiz, A., J. Idkowiak-Baldys, N. Nieto-Rementería, M. D. Boyano, Y. A. Hannun, and A. Asumendi. 2012. Dihydroceramide accumulation and reactive oxygen species are distinct and nonessential events in 4-HPR-mediated leukemia cell death. *Biochem. Cell Biol.* **90**: 209–223.
44. Laviad, E. L., L. Albee, I. Pankova-Kholmyansky, S. Epstein, H. Park, A. H. Merrill, Jr., and A. H. Futerman. 2008. Characterization of ceramide synthase 2: tissue distribution, substrate specificity, and inhibition by sphingosine 1-phosphate. *J. Biol. Chem.* **283**: 5677–5684.

45. Sassa, T., T. Hirayama, and A. Kihara. 2016. Enzyme activities of the ceramide synthases CERS2-6 are regulated by phosphorylation in the C-terminal region. *J. Biol. Chem.* **291**: 7477–7487.
46. Pou, A., J. L. Abad, Y. F. Ordóñez, M. Garrido, J. Casas, G. Fabriàs, and A. Delgado. 2017. From the configurational preference of dihydroceramide desaturase-1 towards Δ^6 -unsaturated substrates to the discovery of a new inhibitor. *Chem. Commun. (Camb.)*. **53**: 4394–4397.
47. Casasampere, M., L. Camacho, F. Cingolani, J. Casas, M. Egidio-Gabás, J. L. Abad, C. Bedia, R. Xu, K. Wang, D. Canals, et al. 2015. Activity of neutral and alkaline ceramidases on fluorogenic N-acylated coumarin-containing aminodiols. *J. Lipid Res.* **56**: 2019–2028.
48. Mao, Z., W. Sun, R. Xu, S. Novgorodov, Z. M. Szulc, J. Bielawski, L. M. Obeid, and C. Mao. 2010. Alkaline ceramidase 2 (ACER2) and its product dihydrosphingosine mediate the cytotoxicity of N-(4-hydroxyphenyl)retinamide in tumor cells. *J. Biol. Chem.* **285**: 29078–29090.
49. Brüning, A., A. Karrenbauer, E. Schnabel, and F. T. Wieland. 1992. Brefeldin A-induced increase of sphingomyelin synthesis. Assay for the action of the antibiotic in mammalian cells. *J. Biol. Chem.* **267**: 5052–5055.
50. Subathra, M., M. Korrapati, L. A. Howell, J. M. Arthur, J. A. Shayman, R. G. Schnellmann, and L. J. Siskind. 2015. Kidney glycosphingolipids are elevated early in diabetic nephropathy and mediate hypertrophy of mesangial cells. *Am. J. Physiol. Renal Physiol.* **309**: F204–F215.
51. Salama, M. F., B. Carroll, M. Adada, M. Pulkoski-Gross, Y. A. Hannun, and L. M. Obeid. 2015. A novel role of sphingosine kinase-1 in the invasion and angiogenesis of VHL mutant clear cell renal cell carcinoma. *FASEB J.* **29**: 2803–2813.
52. Highkin, M. K., M. P. Yates, O. V. Nemirowskiy, W. A. Lamarr, G. E. Munie, J. W. Rains, J. L. Masferrer, and M. M. Nagiec. 2011. High-throughput screening assay for sphingosine kinase inhibitors in whole blood using RapidFire® mass spectrometry. *J. Biomol. Screen.* **16**: 272–277.
53. Salas, A., S. Ponnusamy, C. E. Senkal, M. Meyers-Needham, S. P. Selvam, S. A. Saddoughi, E. Apohan, R. D. Sentelle, C. Smith, C. R. Gault, et al. 2011. Sphingosine kinase-1 and sphingosine 1-phosphate receptor 2 mediate Bcr-Abl1 stability and drug resistance by modulation of protein phosphatase 2A. *Blood.* **117**: 5941–5952.